DOI: 10.24874/ti.2304.07.26.09

Tribology in Industry

www.tribology.rs

RESEARCH

Computational Analysis of Erosion in Savonius Tidal Turbines for Near-Shore Sites

Aerk Dimri[a], Adil Saeed[a], Zulfiqar Ahmad Khan[a,b,c,*]

[a]*Department of Design and Engineering, Bournemouth University, Poole, BH12 5BB, UK,*
[b]*State Key Laboratory of Tribology in Advanced Equipment, Tsinghua University, Beijing 100084, China,*
[c]*Department of Mechanical Engineering, New Uzbekistan University, Tashkent, Uzbekistan.*

Keywords:

Erosion mechanism
Cavitation
Solid particle impingement
Savonius tidal turbine
Near-shore
Low flow
Computational Fluid Dynamics
Discrete phase model

* Corresponding author:

Zulfiqar Ahmad Khan
E-mail: zkhan@bournemouth.ac.uk

Received: 22 July 2026
Revised: 31 August 2026
Accepted: 16 September 2026

A B S T R A C T

Deploying Savonius Tidal Turbines (STTs) in shallow, low-velocity near-shore environments offers a viable alternative to conventional turbines, but their economic feasibility is threatened by erosion from cavitation and Solid Particle Impingement (SPI).

This study analysed STT blade erosion characteristics using a two-step methodology based on Poole Harbour reference data. Global flow behaviour was modelled via 3D transient Computational Fluid Dynamics (CFD), while localised wear hotspots were evaluated using a 2D CFD-Discrete Phase Model (DPM) coupled with the Oka erosion model.

The analysis revealed that STTs face negligible cavitation risk due to low tip-speed ratios, making SPI the primary mode of degradation. Further, unlike high-velocity turbines, maximum abrasive wear on near-shore STTs concentrates near a flow stagnation region due to increased, localised particle impingement. Driven by this stagnation point effect, this erosion is focused on the upstream surface of the returning blade facing away from the centre.

By extending erosion analysis methodologies to low-velocity near-shore STTs, these findings establish an initial spatial mapping framework to identify high-risk wear regions on the blades, helping guide future material reliability and structural durability research for near-shore tidal deployments.

1. INTRODUCTION

Motivated by an increasing focus on sustainability and the need for reliable power generation, tidal energy has been identified as an important source for decarbonising today's energy mix. This is primarily due to its predictability; because tidal currents are governed by celestial mechanics, grid operators can forecast generation years in advance, allowing tidal energy to function similarly to reliable baseload power. Furthermore, because water is significantly denser than air, tidal systems boast a higher energy density than wind energy systems. Consequently, they generate substantial kinetic power from a compact physical space, making the technology uniquely beneficial for coastal and island communities facing spatial constraints while transitioning to clean energy. Finally, tidal energy resources are distributed globally, with recent evaluations identifying hundreds of candidate sites worldwide [1].

In academia and industry, Horizontal Axis Tidal Turbines (HATTs) have emerged as the leading tidal energy technology type, sharing structural similarities with wind turbines and benefiting from years of accumulated industry experience, with some studies showing developmental parallels between the industries [2]. Because most prior research focuses on large-capacity axial-flow turbines designed for deep-water applications, current commercial technologies are being developed for deployment in remote, high-energy offshore environments, leaving shallow-water near-shore environments underutilised [3,4].

Historically, technological development has favoured deep-water sites with high current velocities, such as the UK's Pentland Firth and Italy's Strait of Messina, where peak currents exceed 3.0 m/s [1,5]. However, highly energetic offshore locations are often geographically remote, complicating grid connectivity. Consequently, interest is shifting toward near-shore and shallow-water resources [3]. These coastal environments, including the German North Sea and Malaysia's Malacca Strait, typically feature shallower depths and slower flows averaging 0.8 to 1.0 m/s [4,6]. Recent investigations targeting less energetic near-shore systems highlight the unsuitability of conventional HATTs in these settings, instead proposing the utilisation of Vertical Axis Tidal Turbines (VATTs) and Cross-Flow Turbines (CFTs). These devices scale effectively in constrained depths, offer high power densities, and inherently accommodate bidirectional coastal flows without complex yaw mechanisms, paving the way for cost reductions [3,4].

1.1 Challenges in tidal energy development

A primary challenge in tidal energy development is its economic competitiveness compared to more established renewable technologies, such as wind power. Key factors hindering economic viability include high construction, operation, and maintenance costs driven by logistical difficulties within seawater environments [7]. These financial barriers across both demonstration and commercial-scale deployments, with expenses concentrated in foundation, mooring, and long-term maintenance strategies [8]. Further, the prevailing assumption that power extraction from tidal flows below 2 m/s is uneconomical severely limits the number of geographical locations where tidal energy can be feasibly exploited [9]. These challenges highlight the need to develop modular or reduced-scale turbine designs capable of harnessing low-velocity flows cost-effectively.

Beyond initial capital costs, tidal energy converters must survive continuously in severe marine conditions. To be commercially viable, tidal devices are expected to operate in harsh environments for up to 25 years without needing major maintenance. High-velocity tidal currents are naturally accompanied by high turbulence and severe wave climates, which significantly increase fluctuating loads on turbine blades, resulting in premature device failure and fatigue [10,11]. Furthermore, these currents carry high concentrations of sediments that can cause erosion driven by cavitation and particle impingement. SPI involves suspended sediments, such as sand and silt, repeatedly striking the blade surfaces, leading to abrasive wear and progressive material cutting [11,12]. The severity of this degradation relies heavily on particle characteristics (e.g., size, shape, and hardness) as well as operational impact parameters like impact velocity and angle [11,12]. Conversely, cavitation erosion occurs when local absolute pressure drops below the fluid's vapour pressure at a given operating temperature, causing microscopic vapour bubbles to form and subsequently collapse. This violent bubble collapse produces high-pressure shockwaves and energetic micro-jets that plastically deform the blade surface, creating shallow pits and gradually increasing surface roughness [11].

In sediment-laden environments, these degradation modes rarely act in isolation [11]. Cavitation and solid particle erosion frequently exhibit a compounding impact, where the shockwaves from collapsing cavitation bubbles dramatically accelerate nearby suspended sediment particles into the blade surface. This combined action results in significantly more severe material loss than either mechanism acting independently [12]. Furthermore, frictioninduced adhesive wear generated by shear interactions between the viscous seawater and the blade surface contributes to cumulative material loss over prolonged service [11]. Research shows that the progressive roughening of the blade surface from these erosion mechanisms disrupts the local hydrodynamic flow, induces premature boundary layer transition, increases drag, and reduces lift, leading to a decline in the overall energy conversion efficiency and structural integrity of HATTs [11].

1.2 Research gap

The reviewed literature reveals an imbalance in studying hydrokinetic turbine degradation. While the erosion mechanisms and resulting efficiency losses of high-head hydraulic turbines and HATTs are comprehensively documented [11,12], the quantitative assessment of material wear in VATTs represents an unresolved gap. An overarching theme in the current landscape is the prioritisation of hydrodynamic performance optimisation over long-term structural reliability; studies on Darrieus turbines frequently model cavitation-induced efficiency drops without quantifying material erosion [13], while Savonius turbine research remains almost exclusively confined to static torque and power coefficient parametric studies [14,15]. Further, the fundamental differences between the lift-based and drag-based operation of these turbines mean that these turbines face divergent degradation risks. Specifically, lift-based Darrieus turbines, which share characteristics with HATTs, experience high-velocity cavitation and particle impingement, whereas drag-based Savonius turbines avoid these mechanisms in their low-velocity application [11,15,16].

1.3 Motivation

Collectively, these findings highlight the current focus on turbine performance to assess the feasibility of VATTs and CFTs. These considerations are insufficient when viewed in the context of the 25-year lifespan expected of these devices. To advance the field, research must extend to integrated multiphysics modelling that explicitly correlates site-specific sediment characteristics and operational kinematics with progressive material mass loss in these turbines. Specifically, STTs generate rotational torque by relying on the shape-induced drag difference between the advancing and returning turbine blades. When the tidal current impacts the rotor, it creates a high-pressure region on the upstream surface of the advancing blade and a low-pressure region on the downstream surface. This force imbalance pushes the turbine blade forward, resulting in turbine rotation, as shown in Fig. 2 [17]. Furthermore, studies highlight beneficial characteristics such as superior self-starting, operation independent of flow direction, higher efficiency at low current velocities, maximisation of swept area, a more compact structure, increased flexibility, and potentially greater reliability [17-20]. These advantages make STTs highly suitable for developing simple, low-cost, and scalable near-shore tidal energy generation systems. Hence, the present study aims to analyse and evaluate the turbine blade erosion characteristics of STTs in near-shore conditions. This work extends methodologies currently used to analyse erosion in HATTs to research focused on improving the reliability of STTs and reducing maintenance costs. The geometry used in this study is shown in Fig. 1.

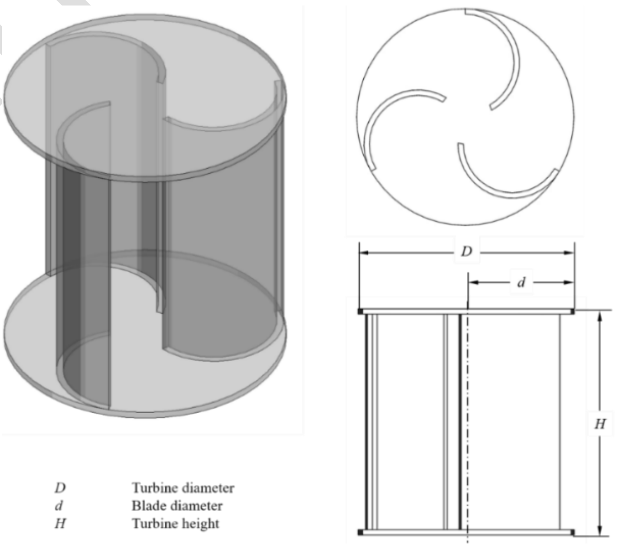

Fig. 1. Savonius turbine geometry.

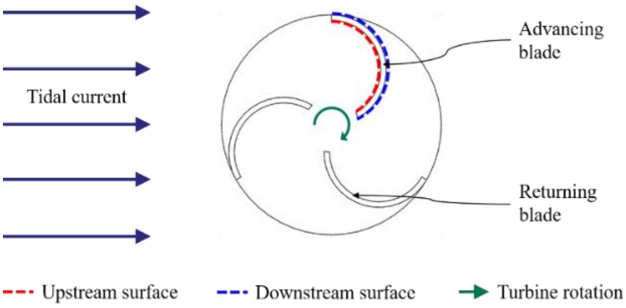

Fig. 2. Savonius turbine operation.

1.4 Present objectives

In view of the above, the present CFD and DPM studies are undertaken with semicircular three-bladed STTs. Additionally, the need for further simulation and testing with various sediment particles has been recognised to address the effect of material hardness on erosion rates. Though this issue has not been addressed here, such studies are essential to provide insight for cost-benefit evaluations affecting economic viability. The lack of such experimentation has led to limited data required for validating the DPM results; however, the obtained results can support observations based on the global and local flow characteristics. Furthermore, this transient DPM study establishes a qualitative spatial framework to identify primary abrasive wear zones driven by SPI, laying the foundation for targeted structural reinforcements (see Section 2.3 regarding Oka model limitations). Overall, the novelty of this investigation lies in characterising the flow over an STT in near-shore conditions to identify the drivers and key regions of erosion. To meet the objectives of this study, a 3D transient CFD simulation using ANSYS Fluent was initially carried out to obtain the flow characteristics, including minimum absolute pressure, fluid velocity, and the STT angular velocity. These velocities were compared to identify regions of erosion driven by either cavitation or SPI. Finally, to gain deeper insight into the primary wear zones, a 2D transient CFD-DPM simulation was conducted to observe the spatial erosion pattern. The investigation strategy for this study is shown in Fig. 3.

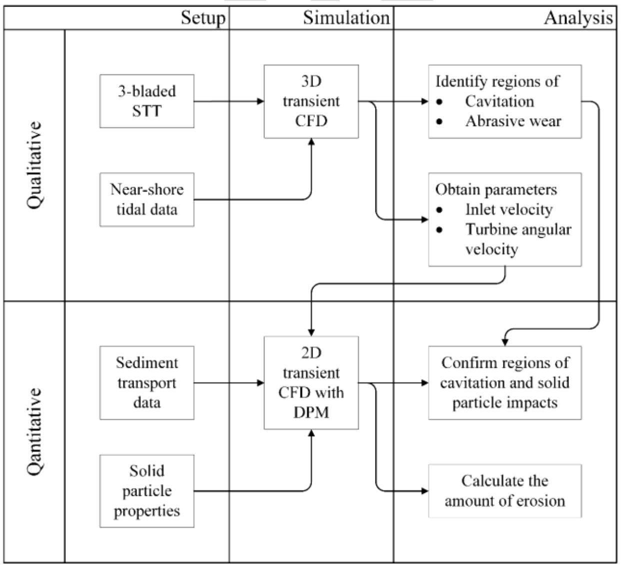

Fig. 3. Adopted methodology of the present study.

1.5 Reference site and physical inputs

To ground the numerical models in a representative coastal environment, boundary conditions and particulate parameters are derived from Poole Harbour, UK, a shallow, sediment-laden estuary serving as a conservative reference site for low-velocity near-shore deployments (Table 1). The model incorporates the turbine geometry (Table 2) and phase material properties (Table 3), utilising pure silica-quartz (SiO_2) as the inert impinging particle. To replicate natural estuarine sediment transport, a non-spherical particle sphericity of 0.6 is applied [21].

Table 1. Poole Harbour reference data.

Parameters	Values	Source
Max. harbour depth	5 m	[22]
Maximum velocity (Entrance)	~ 2 m/s	[23]
Maximum suspended sediments (Severe weather)	600 ppm	
Sediment composition	Fine sand (SiO_2)	[24]
Maximum temperature (September)	17.9 °C	[25]

Table 2. Design specification of the turbine.

Parameters	3 semicircular-bladed STT
Turbine diameter (D)	0.8 m
Blade diameter (d)	0.4 m
Turbine height (H)	0.8 m
Inner diameter (where blades end)	0.2 m
Turbine blade thickness	0.02 m

Table 3. Material properties used.

Material properties	Values	Source
Fluid		
Water-liquid (freshwater from rivers)		
Density	998.2 kg/m^3	
Viscosity	1.003e-03 kg/(m s)	
Vapour pressure at 20°C	2.339 kPa	[26]
Water-salt (seawater)		
Density	1024 kg/m^3	
Viscosity	9.6e-04 kg/(m s)	
Vapour pressure at 20°C (NaCl)	1.768 kPa	[26]
Inert particle		
silica-quartz-fused (SiO^2)		
Density	2194.9 kg/m^3	
Mean grain size	0.25 mm	[24]
Sphericity	0.6	[21]

Source: Density and viscosity values from Ansys® Fluent with MDS 2025 R1

2. METHODS

2.1 Key indicators for analysing erosion

The continuous degradation of tidal turbines is driven by complex, multiphase flow interactions. Predicting and mitigating material loss requires identifying and quantifying the hydrodynamic and particulate metrics discussed below. Evaluating these indicators enables the accurate analysis of both cavitation erosion and abrasive wear, which compromise the structural integrity and operational efficiency of turbine blades [11,12].

Cavitation erosion

Beyond monitoring the simulation domain for regions where the absolute pressure drops below the fluid vapour pressure, the dimensionless cavitation number (σ) is utilised to quantify a flow's susceptibility to cavitate. It defines the margin between the operational absolute and vapour pressures relative to the kinetic energy of the flow, formulated as [27,28]:

$$\sigma = \frac{P - P_v}{0.5\rho V^2} \quad (1)$$

Where P is the reference/ambient local absolute pressure of the fluid (Pa), P_v is the vapour pressure of the fluid at the operating temperature (Pa), ρ is the fluid density (kg/m^3), and V is the characteristic flow velocity (m/s). The greater the cavitation number, the less likely cavitation is to occur.

To model the actual phase-transition process during numerical simulations, transport equations based on volume fractions are employed. The widely utilised Zwart-Gerber-Belamri (ZGB) cavitation model applies the Rayleigh-Plesset equation for bubble dynamics to calculate the specific mass transfer rates between the liquid and vapour phases. Within this theory, evaporation and condensation rates are mathematically derived as functions of the vapour volume fraction, cavitation-core volume fraction, bubble radius, and absolute pressure difference [29,30].

Abrasive particle impact

Unlike cavitation, abrasive SPI is governed by discrete mechanical interactions between suspended sediments and the turbine surface [11]. The severity of this abrasive wear is dictated by material properties (e.g., Brinell or Vickers hardness and density) [12,31], particle characteristics (e.g., size, shape/sphericity, concentration, and mineral hardness) [12,31], and impact kinematics, specifically the particle impact velocity and impingement angle [12,31].

To mathematically predict material removal from abrasive impacts, researchers implement an Eulerian-Lagrangian (E-L) tracking framework paired with empirical erosion models. The continuous fluid phase is resolved first, and the particles are tracked by calculating the drag, buoyancy, pressure gradient, and virtual mass forces acting upon them [16, 31]. Once a particle-wall collision is detected, the impact angle (θ_{imp}) is geometrically determined using the normal vector of the impacted surface (n) and the particle velocity vector (u_p), formulated as [31]:

$$\theta_{imp} = \left| \cos^{-1}\left(\frac{n \cdot u_p}{|n|\,|u_p|}\right) - \frac{\pi}{2} \right| \quad (2)$$

Established erosion models, such as the Oka, Mansouri, or Finnie models, are then applied to calculate local mass loss [12,31]. For example, the Mansouri and Oka models define the erosion rate as a complex function of the target's Brinell hardness (HB), a particle shape factor (F_s), the impact velocity (u_p) raised to an empirically derived velocity exponent (often ~2.41), and a trigonometric function of the impact angle ($f(\theta_{imp})$) [16,28,31].

Because sediment trajectories are heavily influenced by the continuous fluid phase, mapping fluid velocity gradients offers a reliable preliminary method for predicting erosion hotspots. Regions exhibiting intense velocity gradients, high relative flow velocities, or sudden flow separation directly dictate the acceleration and localised concentration of sediment particles [32]. For example, high-velocity crossflows and leakage vortices generated in turbine clearances actively entrain particles, acting as a slingshot that drastically increases local particle impact velocities and collision frequencies against surrounding walls [33]. Consequently, analysing these velocity gradients allows researchers to accurately anticipate the spatial distribution of SPI prior to conducting computationally expensive discrete phase tracking.

2.2 3D CFD simulation

To evaluate global 3D transient hydrodynamics, turbine self-starting torque, and domain-wide cavitation susceptibility, a full-scale 3D CFD model was deployed. The model resolves complex spatial flow features, including radial fluid movement and unsteady wake structures, that dictate global operational kinematics [28,29,34].

Computational methodology

Modelling the complex fluid-structure interactions inherent in turbine operation requires a 3D, pressure-based, transient multiphase CFD approach. Because the interaction between the fluid, sediment particles, and the rotating STT generates a highly unsteady flow field with constantly changing relative positions, transient calculations are essential to model the true physical behaviour[35,36]

The 3D transient hydrodynamics are resolved using a pressure-based solver with a standard k–ϵ turbulence model (Table 4). To establish a conservative baseline for cavitation inception, the domain depth is set to 3 m (accounting for low-tide spring conditions) [37], bringing the local static head closer to the fluid vapour pressure. Furthermore, because predicting progressive erosion requires moving beyond static geometries, a dynamic mesh method is used to capture the flow characteristics more accurately [33,36].

The computational domain and corresponding mesh for the 3D simulation are presented in Fig. 4 and Fig. 5, respectively.

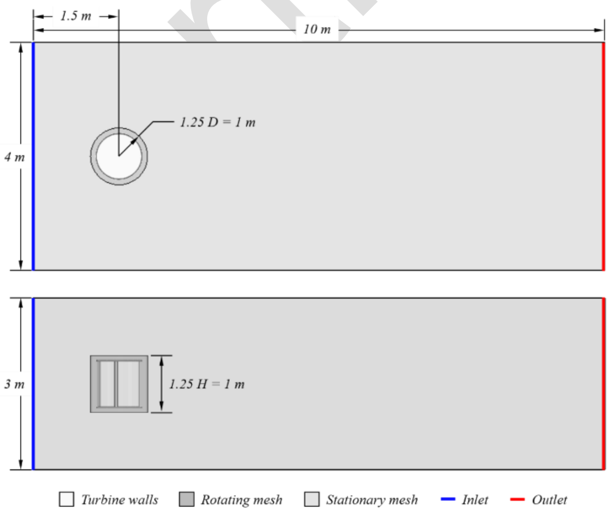

Fig. 4. 3D simulation domain dimensions.

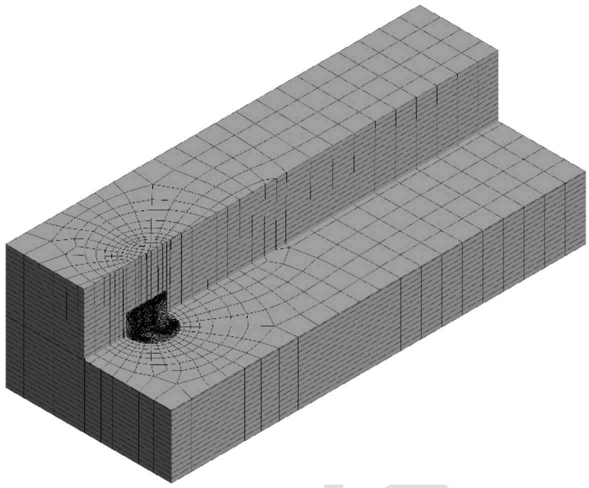

Fig. 5. 3D simulation domain meshing.

Benchmarking

The CFD results for the unresisted, three-bladed semicircular STT at an inlet velocity of 2 m/s align closely with passive-rotation and drag-driven hydrokinetic studies in the literature [17,38,39]. Under zero resisting load, although the time-averaged hydrodynamic torque fluctuates near zero, the system achieves a dynamic angular velocity equilibrium (ω = 4.5 to 4.8 rad/s) and a corresponding tip speed ratio (TSR) of 0.9 to 0.96. These TSR oscillations arise from cyclic force imbalances as the three semicircular blades rotate through 360°, alternating between positive torque on the advancing blades and hydrodynamic drag resistance on the returning blades [17,19,40].

2.3 2D CFD-DPM simulation

To evaluate the spatial distribution and relative intensity of SPI on the turbine blades, a 2D transient simulation was conducted to complement the global 3D flow analysis with high-resolution near-wall particle tracking. In this study, the sediment transport and blade impingement are modelled using the DPM within an E-L framework. This numerical approach is physically and computationally justified by the highly dilute nature of the flow. With a peak suspended sediment concentration of 600 ppm (corresponding to a low volume fraction), particle–particle collisions and the mechanical influence of the discrete phase on the continuous fluid phase are negligible. Consequently, a one-way coupled DPM approach is utilised, providing computational efficiency while capturing high-resolution, near-wall particle trajectories and local collision kinematics necessary to feed the empirical Oka erosion model.

Computational methodology

The localised erosion dynamics are solved using a 2D transient Shear Stress Transport (SST) k–ω turbulence model coupled with Lagrangian DPM particle tracking (Table 4 and Table 5). The SST formulation provides high sensitivity to near-wall boundary layer gradients and adverse pressure separation, which are essential for feeding particle impact kinematics into the Oka model.

Table 4. Comparative specifications of the 3D and 2D simulations.

Configuration	3D Simulation	2D Simulation
Model Purpose & Role	Evaluates global 3D transient flow structures, self-starting torque, and checks for cavitation risk across the domain.	Captures boundary-layer velocity gradients, particle trajectories, and localised erosion hotspots on the blade surface.
Solver Settings	Pressure-Based, Transient.	Pressure-Based, Transient, Double Precision (minimises near-wall truncation errors) [16,31].
Mesh	336,302 cells (748,802 faces, 99,585 nodes).	214,433 cells (429,943 faces, 214,952 nodes).
Turbulence Model	Standard $k{-}\in$ model with Standard Wall Functions.	SST $k-\omega$ model (highly sensitive to wall distance and adverse pressure gradients).
Turbulence Justification	Proven, robust, and stable for bulk-flow patterns and rotating frames in 3D turbomachinery without excessive near-wall refinement overhead [30, 34].	Captures localised flow separation, adverse pressure gradients, and shear stress gradients near the blade surface, vital for near-wall sediment path tracking[12,16,45].
Fluid Domain Properties	Freshwater	Seawater
Inlet Boundary Condition	Transient velocity inlet ramped as $2 \times (1 - e^{-t})$ m/s , which approaches a steady 2 m/s , after $t = 4s$.	Constant velocity inlet of 2 m/s (normal to inlet plane).
Wall Boundary Conditions	No-slip walls for turbine blades and riverbed; Free-slip for sides and top.	No-slip wall for rotor blades; Free-slip for side boundary walls.
Mesh Motion / Rotation	Transient Mesh Motion (sliding mesh). Flow-driven starting rotation from 0 rad/s.	Transient Mesh Motion (sliding mesh). Fixed angular velocity of −4.8 rad/s matching 3D steady state.
Time-Step Size (Δt)	$\Delta t = 0.01$ s (100 max iterations/step)	$\Delta t = 0.0036$ s (80 max iterations/step)
Solver & Residuals	Coupled SIMPLE solver; all residual absolute criteria set to 10^{-3} [28,36,41].	Coupled pressure-velocity solver (robust convergence during complex multiphase momentum exchange) [16]; residual absolute criteria set to 10^{-3}.

Table 5. Setup of the 2D DPM model.

Parameter	Details
Particle Injection Setup	Surface injection normal to inlet; total flow rate = 9.84 kg/s; injected after the continuous flow field stabilises.
Turbulent Dispersion	Stochastic Tracking (Discrete Random Walk model) enabled to capture particle interactions with fluid eddies.
Particle Rebound Model	Reflecting boundary conditions on the turbine; coefficients defined as polynomial functions of impact angle.
Erosion Model & Hardness	Oka Erosion Model; Turbine wall material Vickers Hardness (Hv) = 1.9 GPa.
Oka Empirical Constants	Reference erosion rate = 0.0006154; Velocity exponent = 2.35; Diameter exponent = 0.19; Reference diameter = 0.000326 m; Reference velocity = 104 m/s; Angle constants (n_1 = 0.8, n_2 = 1.3).

To resolve localized erosion without the prohibitive computational overhead of full 3D Lagrangian tracking, the global 3D flow analysis is complemented by a high-resolution 2D planar CFD-DPM framework [31,36,41]. A two-tier numerical methodology is implemented to balance domain-wide hydrodynamic fidelity with localised erosion resolution. First, a 3D transient CFD model evaluates global flow structures, rotational equilibrium, and cavitation risk across the turbine envelope. Second, a 2D CFD-DPM model resolves near-wall boundary layer gradients, permitting dense discrete particle parcel tracking and precise impact kinematic inputs for the Oka erosion model [12,16,31,41]. The computational domain, along with the meshing for the 2D simulation, is shown in Fig. 6.

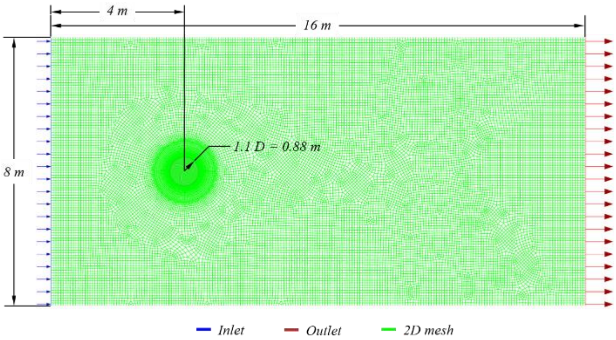

Fig. 6. 2D simulation domain dimensions and meshing.

Mesh size and y^+ values

To ensure adequate near-wall grid resolution along the rotating turbine blades, a structured boundary layer mesh was generated using an edge element sizing of 0.003 m, supplemented by 7 inflation layers with a 1.2 geometric growth rate. Given the complex kinematics of the vertical axis wind turbine, the local flow field experiences large periodic variations, causing the maximum $y+$ values to fluctuate cyclically between approximately 75 and 130 in steady operation. This is due to the variations in relative velocity and effective angle of attack as the blade moves through the upstream and downstream sectors. Conversely, the minimum $y+$ values remain close to zero. Because the values span both the log-law region and the viscous sublayer temporally and spatially, the use of the SST $k-\omega$ model is suitable for implementation in ANSYS Fluent, which uses an automatic wall treatment switching between low-Reynolds number formulations and standard wall functions [42] to preserve numerical stability while capturing complex flow characteristics.

Selecting the Oka erosion model and its limitations

The Oka erosion model is a mathematically robust empirical formula designed to predict progressive material removal from discrete particle impacts [12,31]. Implementing this model within a 2D CFD-DPM framework for an STT is highly advantageous; the computationally efficient 2D domain allows for fine near-wall mesh resolutions, which are essential for accurately calculating localised particle impact velocities and geometric impingement angles [31,36,41].

The Oka model uniquely capitalises on these high-fidelity collision kinematics, defining the localised erosion rate as a function of target material hardness, particle shape, impact velocity, and an impact angle function [16,31]. Because STT blades feature continuously curving profiles, suspended particles strike the surface at varying trajectories. The Oka model's inclusion of an impact angle function accurately accounts for the transition between shallow-angle cutting wear and normal-angle plastic deformation, making it exceptionally well-suited for evaluating spatial degradation on curved turbine blades [12,16,31].

Despite its advantages, coupling the Oka model with high-resolution DPM tracking is constrained by its reliance on empirical constants [11,12]. Derived from controlled laboratory settings, these constants frequently fail to replicate the complex operating conditions of full-scale hydrokinetic turbines [12].

To accurately calibrate empirical erosion models like the Oka model for specific turbine architectures, targeted experimental testing must closely replicate actual hydrodynamic and environmental conditions. Standard laboratory setups are often insufficient, necessitating a specialised testing methodology. Testing will need to utilise a scaled-down model turbine test rig designed to simulate the specific flow velocities and operating conditions of the intended deployment site, as jet-type or slurry pot erosion testers may not sufficiently capture complex fluid motion [12,43]. Further, the experimental sediment must precisely match the physical properties of the deployment site, including density, mineral composition (hardness), median particle size, and concentration [35,44]. As particles continuously strike the turbine, they lose angularity and break down, artificially reducing the erosion rate over time [12]. To maintain calibration accuracy, researchers must either implement an open-loop system with a continuous fresh sediment supply or replace the sediment at fixed intervals [12].

Because the empirical constants of the Oka model are derived under controlled laboratory conditions, they do not replicate full-scale hydrokinetic operating environments. Consequently, the lack of such targeted experimentation on STTs results in limited data for the direct quantitative validation of DPM mass-loss predictions [33]. However, the model reliably provides a qualitative spatial framework identifying erosion hotspots, shielding effects, and spatial erosion patterns correlating with local velocity gradients and high-concentration particle trajectories [16,33,41].

Boundary conditions

Because SPI is governed by relative impact kinematics, the 2D simulation models the continuous operating phase where the velocity difference between the tidal current and the returning blade peaks (Fig. 7).

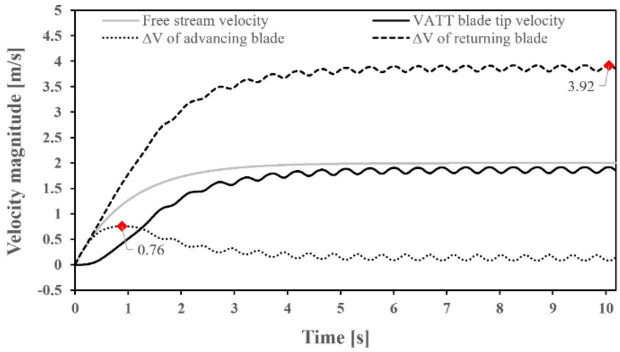

Fig. 7. Tidal current and turbine blade velocity characteristics and points of maximum velocity difference.

This setup uses a constant angular velocity of 4.8 rad/s, derived from the steady 3D flow-driven simulation (Table 4). While this simplification neglects transient, cyclic rotational speed fluctuations caused by drag-based torque variations, it captures cumulative spatial wear patterns over multiple revolutions and averages out the micro-peaks associated with instantaneous particle impacts at higher rotational speeds. Furthermore, although the 2D planar framework ignores the 3D axial spilling of fluid over the blade tips, artificially increasing near-wall velocities and introducing a conservative over-predictive bias in erosion magnitudes, it ensures complete numerical stability and reliably identifies primary wear hotspots on the returning blade.

Furthermore, the 2D CFD-DPM simulation is not presented as a direct quantitative validation of the 3D flow model. Instead, the 2D model functions as a highly refined, complementary, localised erosion-tracking tool. The continuous fluid phase properties in the 3D and 2D simulations are tailored to represent distinct case limits: the 3D hydrodynamic model utilises fresh water properties as a baseline for torque generation, whereas the 2D erosion model utilises saltwater and fine sand properties (Table 3) to reflect the denser, more corrosive estuarine environment of Poole Harbour.

3. RESULTS AND DISCUSSION

3.1 Very low risk of cavitation in STTs

The 3D CFD simulation results show that the minimum local absolute pressure in the simulation domain throughout the start-up and steady operating phases is 95.87 kPa, with a local characteristic velocity of 4.2 m/s. This minimum absolute pressure is much larger than the available vapour pressures of 2.34 kPa and 1.77 kPa from Table 3. The minimum absolute pressure over time is summarised in Fig. 8. Substituting the obtained values in Equation 1 yields a cavitation number of $\sigma_1 = 10.62$ for freshwater $(\rho_1 = 998.2\ \mathrm{kg/m^3}, P_{v1} = 2.34\ \mathrm{kPa})$ and $\sigma_2 = 10.42$ for seawater $(\rho_2 = 1024\ \mathrm{kg/m^3}, P_{v2} = 1.77\ \mathrm{kPa})$. Because both values are over an order of magnitude greater than the critical threshold for incipient cavitation $(\sigma_{\mathrm{crit}} \approx 1.0)$ cavitation inception is physically ruled out. For comparison, Fan et al. observed only minor tip vortex cavitation at a much lower cavitation number of 5.45 for a HATT at a Tip-Speed Ratio (TSR) of 3 [29], whereas STTs generally operate at a lower TSR. This helps STTs avoid the scale-induced cavitation issues frequently reported in the literature as TSRs increase [11,29].

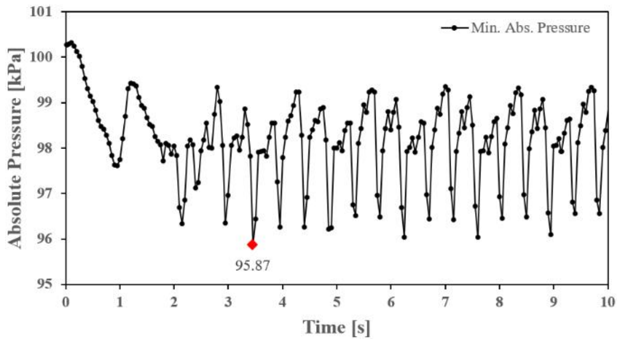

Fig. 8. Minimum absolute pressure in the simulation domain over time.

However, deploying these turbines in sediment-laden near-shore sites introduces solid particle and fluid dynamics interactions that may contradict clean-water simulations. Literature indicates that the entrainment of sediment particles can increase the size, number, and distribution of cavitation nuclei. This phenomenon alters local pressure distributions and enhances cavitation, suggesting that the current simulated pressures may underestimate the true cavitation risk in abrasive, multiphase environments [12,34].

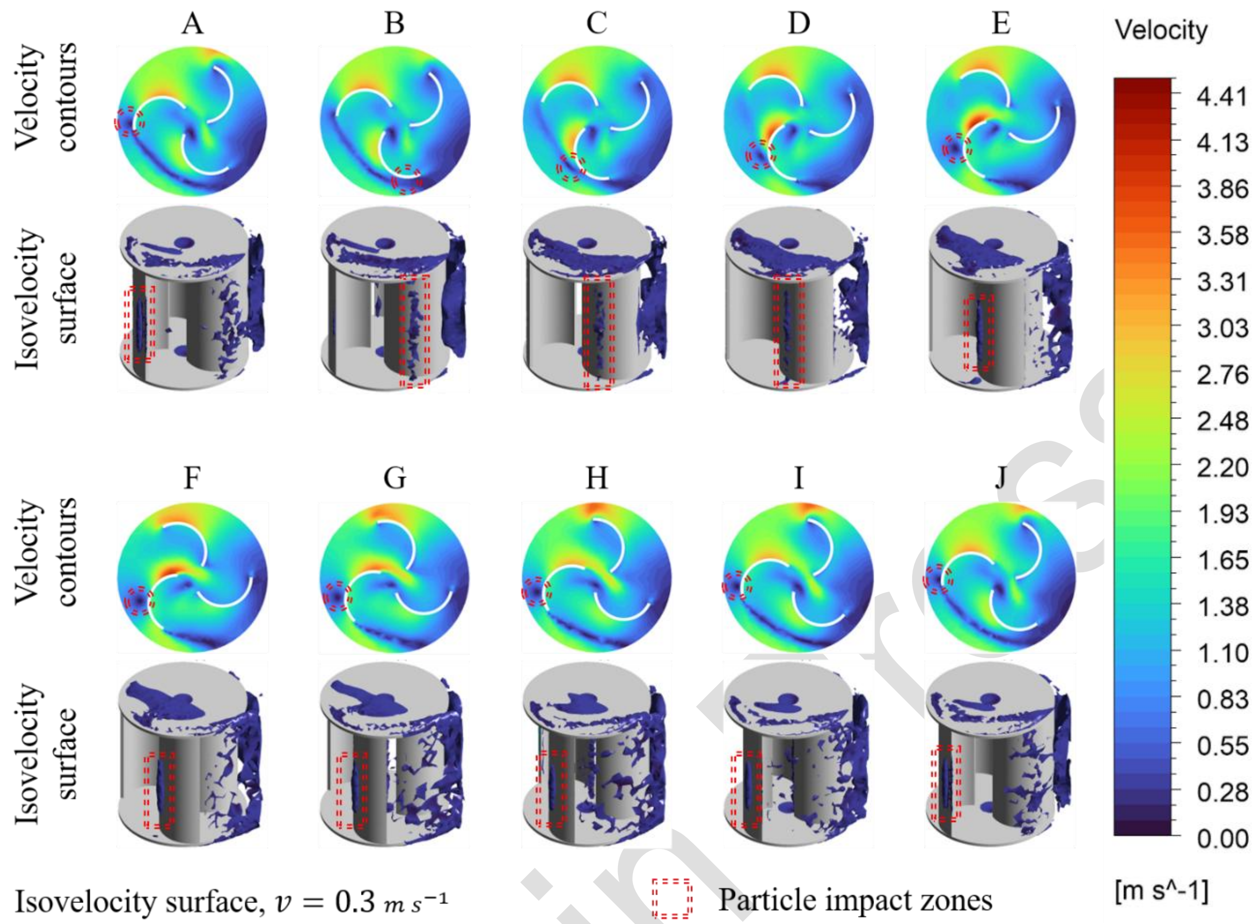

Fig. 9. Low velocity regions suggesting SPI zones on the returning blade of a Savonius tidal turbine.

3.2 Regions susceptible to SPI

The 3D CFD simulation results highlight core low-velocity zones utilising isovelocity surfaces where the tidal current velocity approaches 0.3 m/s near the STT walls, suggesting a high likelihood of SPI in these regions. These predicted impact zones are illustrated in Fig. 9 and reveal two primary areas susceptible to abrasive erosion:

- The upstream surface of the returning blade, where low-velocity zones suggest concentrated erosion away from the turbine's centre.
- The endplate. Although evaluating this area falls outside the current scope, investigating it remains essential to understand total erosion rates and blockage effects across the complete turbine assembly.

3.3 SPI-driven erosion

The 2D CFD-DPM simulation results confirm that maximum SPI erosion occurs in the previously identified low-velocity impact zones near the STT blade walls. Over a tracking duration of 15 seconds (representing 11.46 complete turbine revolutions at a rotational velocity of 4.8 rad/s, which ensures a periodically stable particle-impact pattern), the simulation records an integrated, accumulated local mass loss per unit area of 3.06×10^{-8} kg/m^2. As noted in Section 2.3, uncalibrated empirical constants mean this numerical figure serves as a qualitative spatial indicator of erosion rather than a physical field degradation rate. The spatial distribution of this accumulated wear is presented in Fig. 10.

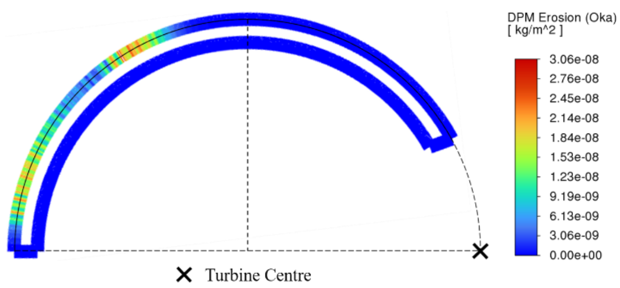

Fig. 10. Spatial distribution of accumulated local mass loss per unit area (kg/m^2) on a three-bladed Savonius rotor after a 15-second DPM simulation.

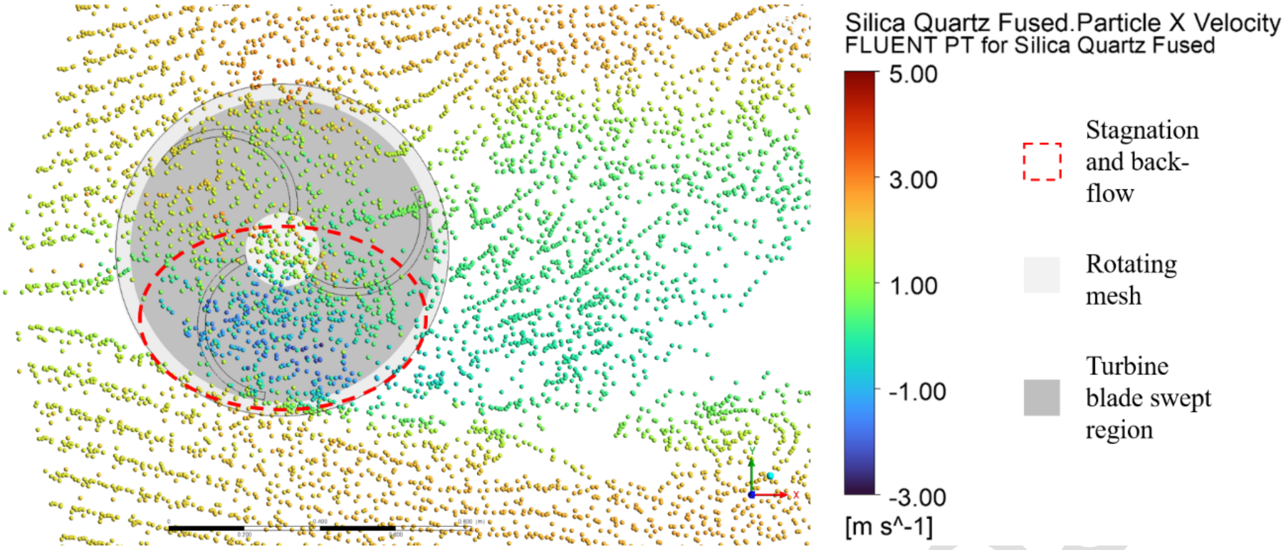

Fig. 11. Visualising the stagnation point zones in STTs using particle X velocity tracking.

Because the sediment phase is dilute and governed by one-way coupling, a linear scaling relationship exists between the sediment mass concentration and the resulting material wear rates. Furthermore, since the spatial distribution of particle collision trajectories and impact angles is governed by the developed fluid flow field, the identified wear hotspots on the upstream surface of the returning turbine blade in this study may be applied across all flow conditions. Under typical, calm, continuous-operation states, only the magnitude of the accumulated mass loss is expected to reduce linearly while retaining the characteristic spatial erosion. This linear sensitivity allows the qualitative erosion maps developed in this study to be scaled predictably across any operational sediment concentration.

The identification of particle impact zones and the localised erosion hotspot evaluation using the 2D CFD-DPM approach coupled with the Oka erosion model align with established numerical methodologies in the literature. Specifically, the concentration of erosion near these stagnation regions is governed by the deceleration of the fluid phase as it approaches the solid boundary similar to observations in a sediment study of a Francis turbine [16]. While local fluid velocity drops, high-inertia particles decouple from the decelerating streamlines, culminating in a highly concentrated localised particle mass flux and high-frequency wall collisions [16]. This stagnation zone is identified using particle X-velocity tracking Fig. 11.

The conclusion that maximum erosion occurs near flow stagnation regions diverges from the broader consensus in hydrokinetic turbine literature, which consistently identifies high impact velocity as the primary driver of severe abrasive wear. Specifically, prior research asserts that:

- Erosion velocity is the dominant factor affecting wear, meaning maximum hydro-abrasive erosion corresponds directly to regions of maximum flow velocity [12].
- The leading edge of a blade is the most likely to experience particle impingement due to higher local velocities [11].
- Degradation rates are accelerated when fluid velocity increases due to a corresponding increase in the cutting and plastic deformation components of the impact [34].

Despite this consensus, these prior studies focus exclusively on high-velocity applications, contrasting heavily with the operational profile of STTs. Consequently, this localised stagnation-driven impingement mechanism represents a unique wear pattern characteristic of STT systems.

4. CONCLUSION

The primary objective of this study was to evaluate the turbine blade erosion characteristics of STTs operating in shallow-water, near-shore environments to improve device reliability and mitigate long-term maintenance costs. This objective was achieved using a tiered numerical methodology with Poole Harbour as a representative low-velocity case study. First, a 3D transient CFD simulation was utilised to capture global flow characteristics and pressure distributions. Subsequently, a computationally efficient 2D CFD-DPM simulation, paired with the Oka erosion model, was applied to identify the spatial distribution of localised abrasive wear driven by discrete sediment impacts.

4.1 Main takeaways

The numerical analysis revealed the following main takeaways and distinct degradation behaviours for STTs compared to traditional axial-flow systems:

- STTs operate with a highly reduced risk of cavitation, maintaining absolute pressures well above the fluid's vapour pressure due to their fundamentally lower TSRs. Consequently, STT erosion in near-shore environments is predominantly driven by SPI rather than cavitation.
- While existing literature on high-velocity hydrokinetic turbines asserts that maximal erosion correlates with peak flow velocities, this study found the opposite to be true for near-shore STT applications.
- SPI and resulting mass loss were concentrated within flow stagnation regions where local fluid velocity drops to zero. Driven by this stagnation point effect, highly concentrated particle impingement and high collision frequencies compensate for local fluid deceleration, leading to significant localised erosion on the upstream surface of the returning blade (specifically facing away from the turbine centre).

4.2 Practical and theoretical implications and limitations

These findings offer significant practical and theoretical implications along with specific limitations:

- Theoretical Implications: These findings depart from the generalised consensus regarding hydro-abrasive wear in high-velocity applications, establishing that low-velocity near-shore STTs experience fundamentally different spatial erosion patterns. Identifying flow stagnation points as the primary sites of degradation provides a tailored framework for predicting STT lifespan.
- Practical Implications: Mapping localised wear tendencies along the returning blade provides a geometric guide for future structural optimisation or targeted blade coating applications. Demonstrating that STTs inherently resist cavitation under these conditions provides a useful baseline for future multi-year fatigue and comprehensive techno-economic feasibility studies of near-shore deployments.
- Limitations: Without direct experimental calibration for the Oka model constants under these flow conditions (Section 2.3), absolute mass-loss predictions cannot project real-world service life. These wear maps must be interpreted strictly as qualitative geometric indicators of erosion susceptibility.

4.3 Future work

To build upon this work, future research should prioritise the following actionable paths:

- Conduct physical experimental testing with various sediment particles to quantify the precise effect of target material hardness on STT erosion rates, which is necessary to validate DPM mass-loss results for cost-benefit analyses.
- Expand 3D simulations to include the full turbine assembly, specifically addressing erosion on the endplates and the resulting blockage effects.
- Develop integrated multiphase models that simultaneously couple discrete solid particle tracking with chemical corrosion and sediment-enhanced cavitation to better simulate real-world marine degradation.

Declarations

No Conflict of Interest

The author(s) declare no conflicts of interest with respect to the research, authorship, and/or publication of this work.

Use of AI tools

In the preparation of this work, the author(s) used Google Gemini to improve the readability and language of the work. After using this tool, the author(s) reviewed and edited the content and take(s) full responsibility for the content of this work.

REFERENCES

[1] D. S. Coles *et al.*, "A review of global tidal stream energy resources," *Proceedings of the Royal Society a Mathematical Physical and Engineering Sciences*, vol. 481, no. 2328, Dec. 2025, doi: 10.1098/rspa.2024.0841.

[2] S. Walker and P. R. Thies, "A review of component and system reliability in tidal turbine deployments," *Renewable and Sustainable Energy Reviews*, vol. 151, p. 111495, Jul. 2021, doi: 10.1016/j.rser.2021.111495.

[3] A. Roberts, B. Thomas, P. Sewell, Z. Khan, S. Balmain, and J. Gillman, "Current tidal power technologies and their suitability for applications in coastal and marine areas," *Journal of Ocean Engineering and Marine Energy*, vol. 2, no. 2, pp. 227–245, Mar. 2016, doi: 10.1007/s40722-016-0044-8.

[4] M. W. A. Rahim, A. A. Rahman, M. Izham, and N. A. M. Amin, "Tidal Energy in Malaysia: An overview of potentials, device suitability, issues and outlook," *Regional Studies in Marine Science*, vol. 61, p. 102853, Feb. 2023, doi: 10.1016/j.rsma.2023.102853.

[5] T. M. El-Geziry, I. G. Bryden, and S. J. Couch, "Environmental impact assessment for tidal energy schemes: an exemplar case study of the Strait of Messina," *Journal of Marine Engineering & Technology*, vol. 8, no. 1, pp. 39–48, Jan. 2009, doi: 10.1080/20464177.2009.11020217.

[6] A. Korte, C. Windt, and N. Goseberg, "Review and assessment of the German tidal energy resource," *Journal of Ocean Engineering and Marine Energy*, vol. 10, no. 1, pp. 239–261, Dec. 2023, doi: 10.1007/s40722-023-00309-7.

[7] H. Akimoto, K. Tanaka, and K. Uzawa, "A conceptual study of floating axis water current turbine for low-cost energy capturing from river, tide and ocean currents," *Renewable Energy*, vol. 57, pp. 283–288, Mar. 2013, doi: 10.1016/j.renene.2013.02.002.

[8] R. O'Connell *et al.*, "The integration of tools for the Techno-Economic evaluation of fixed and floating tidal energy deployment in the Irish Sea," *Energies*, vol. 16, no. 22, p. 7526, Nov. 2023, doi: 10.3390/en16227526.

[9] B. T. Tarver, J. C. L. Chan, and C.-H. Jo, "A new concept in tidal turbines," *International Journal of Energy Research*, vol. 40, no. 5, pp. 579–586, Oct. 2015, doi: 10.1002/er.3440.

[10] L. Perez, R. Cossu, A. Grinham, and I. Penesis, "Datasets for turbulence characterization collected with AD2CPs in potential tidal energy sites in Australia," *Data in Brief*, vol. 43, p. 108336, Jun. 2022, doi: 10.1016/j.dib.2022.108336.

[11] P. Habibi, F. Abad, S. Dai, A. Mehmanparast, and S. Lotfian, "Failure analysis of tidal turbine blades: understanding erosion mechanisms and their impact on structural integrity," *Engineering Failure Analysis*, vol. 182, p. 110045, Aug. 2025, doi: 10.1016/j.engfailanal.2025.110045.

[12] N. Shrivastava and A. K. Rai, "Hydro-abrasive erosion in Pelton turbines: Comprehensive review and future outlook," *Renewable and Sustainable Energy Reviews*, vol. 207, p. 114957, Oct. 2024, doi: 10.1016/j.rser.2024.114957.

[13] O. Lévesque and G. Dumas, "Cavitation study of H-Darrieus hydrokinetic turbines via numerical simulations," *Energy Reports*, vol. 9, pp. 226–239, Oct. 2023, doi: 10.1016/j.egyr.2023.09.150.

[14] M. Syukri. M. Shamsuddin, N. M. Kamaruddin, and Z. Mohamed-Kassim, "The influence of material on the power performance of Savonius turbines in wind and water applications," *Ocean Engineering*, vol. 266, p. 112638, Oct. 2022, doi: 10.1016/j.oceaneng.2022.112638.

[15] M. H. M. Yazik, M. H. Zawawi, A. N. Ahmed, L. M. Sidek, H. Basri, and F. Ismail, "One-way fluid structure interaction analysis of a static savonius hydrokinetic turbine under different velocity and surface roughness with different blade materials," *Ocean Engineering*, vol. 291, p. 116373, Nov. 2023, doi: 10.1016/j.oceaneng.2023.116373.

[16] X.-Y. Wei, X.-F. Kang, J. Pei, and W.-Q. Wang, "Sediment erosion of Francis turbine with splitter blades," *International Journal of Mechanical Sciences*, vol. 304, p. 110674, Jul. 2025, doi: 10.1016/j.ijmecsci.2025.110674.

[17] M. Samadi, M. G. Hassanabad, and S. B. Mozafari, "Performance enhancement of low speed current savonius tidal turbines through adding semi-cylindrical deflectors," *Ocean Engineering*, vol. 259, p. 111873, Jul. 2022, doi: 10.1016/j.oceaneng.2022.111873.

[18] E. Ghamati, H. Kariman, and S. Hoseinzadeh, "Experimental and computational fluid dynamic study of water flow and submerged depth effects on a tidal turbine performance," *Water*, vol. 15, no. 13, p. 2312, Jun. 2023, doi: 10.3390/w15132312.

[19] B. Wang, X. Bai, G. Lei, W. Zhang, and R. Ji, "Effect analysis of the V-Angle and straight edge length on the performance of V-Shaped blades for a Savonius hydrokinetic turbine," *Journal of Marine Science and Engineering*, vol. 13, no. 7, p. 1240, Jun. 2025, doi: 10.3390/jmse13071240.

[20] P. K. Stansby and P. Ouro, "Modelling marine turbine arrays in tidal flows," *Journal of Hydraulic Research*, vol. 60, no. 2, pp. 187–204, Feb. 2022, doi: 10.1080/00221686.2021.2022032.

[21] C. Friz, D. Felix, F. M. Evers, and R. M. Boes, “Predicting field calibration factors for suspended sediment monitoring based on particle size and shape,” *Journal of Environmental Management*, vol. 401, p. 128708, Feb. 2026, doi: 10.1016/j.jenvman.2026.128708.

[22] "i-Boating: Free Marine Navigation Charts & Fishing Maps," *GPS Nautical Charts.* [Online]. Available: https://fishing-app.gpsnauticalcharts.com/i-boating-fishing-web-app/fishing-marine-charts-navigation.html?title=England+-+South+Coast+-+Poole+Harbour+and+Approaches+boating+app#13.27/50.7139/-1.9928. (Accessed: 27 April, 2025.)

[23] "Poole Harbour," *River and Coastal Environments Research*. [Online]. Available: https://www.scopac.org.uk/scopac_sedimentdb/pharb/pharb.htm#intro. (Accessed: 27 April, 2025.)

[24] X.-T. Ong, "Hydrodynamic controls on nearshore sediment sizes in Poole Bay," MSc, Faculty of Engineering and the Environment, University of Southampton, U.K. 2019. [Online]. Available: https://southerncoastalgroup-scopac.org.uk/wp-content/uploads/2020/01/Hydrodynamic-controls-on-nearshore-sediment-sizes-in-Poole-Bay_Xue-Ting-Ong_330579864_01_0000486198_Final-Report.pdf. (Accessed: 27 April, 2025.)

[25] "Poole Sea Temperature" *SeaTemperature.org*. [Online]. Available: https://www.seatemperature.org/europe/united-kingdom/poole.htm. (Accessed Jul. 13, 2026).

[26] "Vapor pressure of saturated salt solutions," in *CRC Handbook of Chemistry and Physics, Internet Version 2005*, D. R. Lide Ed. Boca Raton, FL: CRC Press, 2005, pp. 6-105.

[27] B. Pouffary, "Numerical Modelling of Cavitation," in *Design and Analysis of High Speed Pumps*, Educational Notes, vol. RTO-EN-AVT-143, Paper 3. Neuilly-sur-Seine, France: NATO Research and Technology Organisation, 2006, pp. 3-1–3-54. [Online]. Available: https://publications.sto.nato.int/publications/STO%20Educational%20Notes/RTO-EN-AVT-143/EN-AVT-143-03.pdf. (Accessed Jul. 13, 2026).

[28] Y. Gao, J. Bai, W. Chen, D. Liu, and Y. Lin, “Blade optimization of a tidal current turbine against abrasive wears and cavitation erosion: A numerical and experimental study,” *Ocean Engineering*, vol. 359, p. 126066, May 2026, doi: 10.1016/j.oceaneng.2026.126066.

[29] M. Fan, L. Xu, Z. Hong, C. Han, and Z. Sun, “Cavitation phenomenon and noise characteristics of the tidal current turbine with leading-edge tubercles,” *Renewable Energy*, vol. 256, p. 124400, Sep. 2025, doi: 10.1016/j.renene.2025.124400.

[30] H. Wang *et al.*, “Analysis on cause of erosion of guide vane of high-head Francis turbine in sandy river,” *Energy Science & Engineering*, vol. 12, no. 9, pp. 3704–3717, Jul. 2024, doi: 10.1002/ese3.1838.

[31] Y. Xiao, B. Guo, A. K. Rai, J. Liu, Q. Liang, and J. Zhang, “Analysis of hydro-abrasive erosion in Pelton buckets using a Eulerian-Lagrangian approach,” *Renewable Energy*, vol. 197, pp. 472–485, Jul. 2022, doi: 10.1016/j.renene.2022.07.087.

[32] J. Yang, C. Peng, C. Li, X. Liu, J. Liu, and Z. Wang, “Design and verification of Francis turbine working in sand laden hydro-power plant,” *Renewable Energy*, vol. 207, pp. 40–46, Feb. 2023, doi: 10.1016/j.renene.2023.02.088.

[33] Z. Zhao, Z. Qian, O. G. Dahlhaug, and Z. Guo, “Effect of leakage flow on sediment erosion in guide vane region,” *International Journal of Mechanical Sciences*, vol. 291–292, p. 110122, Mar. 2025, doi: 10.1016/j.ijmecsci.2025.110122.

[34] T. Kashyap *et al.*, “Silt erosion and cavitation impact on hydraulic turbines performance: An in-depth analysis and preventative strategies,” *Heliyon*, vol. 10, no. 8, p. e28998, Apr. 2024, doi: 10.1016/j.heliyon.2024.e28998.

[35] J. Liu *et al.*, “Research on the mechanism of sediment erosion in the bucket of a large-scale Pelton turbine at a hydropower station,” *Powder Technology*, vol. 455, p. 120805, Feb. 2025, doi: 10.1016/j.powtec.2025.120805.

[36] X. Ge *et al.*, “Experimental and Numerical studies on Opening and Velocity Influence on Sediment Erosion of Pelton Turbine Buckets,” *Renewable Energy*, vol. 173, pp. 1040–1056, Apr. 2021, doi: 10.1016/j.renene.2021.04.072.

[37] E. Bamford. "Poole Harbour tides - in depth," *Sailing Today*. [Online]. Available: https://www.sailingtoday.co.uk/cruising/marinas/poole-harbour-tides/. (Accessed Sep. 10, 2026.

[38] Z. Liu, H. Qu, and H. Shi, “Numerical Study on Self-Starting Performance of Darrieus Vertical Axis Turbine for Tidal stream Energy Conversion,” *Energies*, vol. 9, no. 10, p. 789, Sep. 2016, doi: 10.3390/en9100789.

[39] S. Singha and R. P. Saini, “Performance analysis of a modified Savonius hydrokinetic turbine,” *Springer Proceedings in Mathematics & Statistics*, pp. 377–392, Jan. 2020, doi: 10.1007/978-981-15-1338-1_28.

[40] P. Marsh, D. Ranmuthugala, I. Penesis, and G. Thomas, “The influence of turbulence model and two and three-dimensional domain selection on the simulated performance characteristics of vertical axis tidal turbines,” *Renewable Energy*, vol. 105, pp. 106–116, Dec. 2016, doi: 10.1016/j.renene.2016.11.063.

[41] R. Tarodiya, S. Khullar, and A. Levy, "Particulate flow and erosion modeling of a Pelton turbine injector using CFD-DEM simulations," *Powder Technology*, vol. 399, p. 117168, Feb. 2022, doi: 10.1016/j.powtec.2022.117168.

[42] ANSYS, Inc., "Automatic near-wall treatment for omega-based models," in *CFX-Solver Modeling Guide*, sec. 4.2.3, 2026.

[43] N. Arora, A. Kumar, and S. K. Singal, "Technological advancement in measurements of suspended sediment and hydraulic turbine erosion," *Measurement*, vol. 190, p. 110700, Jan. 2022, doi: 10.1016/j.measurement.2022.110700.

[44] B. Qin *et al.*, "Advanced high-precision methodology for assessing sediment erosion in Pelton turbine buckets," *Energy Science & Engineering*, vol. 12, no. 12, pp. 5410–5417, Nov. 2024, doi: 10.1002/ese3.1899.

[45] B. Yao *et al.*, "Effect of sediment erosion on pressure pulsations in a large Pelton turbine," *Energy Science & Engineering*, vol. 12, no. 10, pp. 4040–4056, Sep. 2024, doi: 10.1002/ese3.1858.